NMR Chemical Shift Analysis Decodes Olefin Oligo- and Polymerization Activity of d^0 Group 4 Metal Complexes

Christopher P. Gordon[a], Satoru Shirase[a,b], Keishi Yamamoto[a], Richard A. Andersen,[c,]* Odile Eisenstein,[d,e,]* Christophe Copéret[a,]*

Affiliations

[a] Department of Chemistry and Applied Biosciences, ETH Zürich, Vladimir Prelog Weg 1-5, 8093, Zürich, Switzerland.

[b] Department of Chemistry, Graduate School of Engineering Science, Osaka University, Toyonaka, Osaka 560-8531, Japan

[c] Department of Chemistry, University of California, Berkeley, California 94720, United States.

[d] Institut Charles Gerhardt, UMR 5253 CNRS-UM-ENSCM, Université de Montpellier, 34095 Montpellier, France.

[e] Hylleraas Centre for Quantum Molecular Sciences, Department of Chemistry, University of Oslo, P.O. Box 1033, Blindern, 0315 Oslo, Norway.

Corresponding authors

* Richard A. Andersen, raandersen@lbl.gov
* Odile Eisenstein, odile.eisenstein@univ-montp2.fr
* Christophe Copéret, ccoperet@ethz.ch

Keywords

Olefin Polymerization, Olefin Oligomerization, NMR Spectroscopy, Chemical Shift Tensor Analysis, Frontier Molecular Orbitals, DFT/ZORA Calculations

Abstract

d^0 Metal alkyl complexes (M = Ti, Zr, and Hf) show specific activity and selectivity in olefin polymerization and oligomerization depending on their ligand set and charge. Here, we show by a combined experimental and computational study that the ^{13}C NMR chemical shift tensors of the α-carbon of metal-alkyls, that undergo olefin insertion, signal the presence of partial alkylidene character in the metal-carbon bond, which facilitates this reaction. The alkylidene character is traced to the π-donating interaction of a filled orbital on the alkyl group with an empty low-lying metal d-orbital of appropriate symmetry. This molecular orbital picture establishes a connection between olefin insertion into a metal-alkyl bond and olefin metathesis, and a close link between the Cossee-Arlmann and Green-Rooney polymerization mechanisms. The ^{13}C NMR chemical shifts, the α-H agostic interaction, and the low activation barrier of ethylene insertion are therefore the results of the same orbital interactions, thus establishing chemical shift tensors as a descriptor for olefin insertion.

Significance Statement

The rational understanding and design of catalysts poses a major challenge to the community of chemists. While catalysts are involved in around 90% of all industrial chemical processes, their discovery and development is usually based on massive screening and often serendipity. Here, we show through a detailed analysis of the NMR chemical shift that the activity of olefin polymerization and oligomerization catalysts is directly related to the chemical shift of the carbon atom bound to the metal center. This relation is traced back to specific frontier molecular orbitals, which induce π-character in the metal-alkyl bond, thereby favoring insertion. This result not only reveals a surprising analogy between olefin polymerization and olefin metathesis, but also establishes chemical shift as a descriptor of predictive value for catalytic activity in these industrially relevant processes.

Introduction

Oligomerization and polymerization processes are a highly active field of research (1-5) and at the heart of the petrochemical industry, producing α-olefins and polyolefins, respectively, that are some of the most important commodity chemicals and polymers (6). In polymerization, the coordination and insertion of an olefin into a metal–carbon bond, referred to as the Cossee-Arlmann mechanism, are the key elementary steps for the polymer chain growth process (Fig. 1a) (7-11). To be operative, this mechanism requires electrophilic metal centers, typically in a cationic form, with an empty coordination site (12-16). Neutral metal-alkyl complexes are typically less efficient at inserting olefins, in sharp contrast to the corresponding metal-hydrides (17). In the alternative Green-Rooney mechanism, chain growth has been proposed to involve alkylidene species, formed by α-H transfer from a metal-alkyl species. In this case, the carbon-carbon bond formation takes place via a [2+2]–cycloaddition yielding a metallacyclobutane intermediate (Fig. 1b) (7-8, 18-19). This mechanism is postulated for the formation of polyethylene with $Ta(=CHtBu)(H)I_2(PMe_3)_3$ (20). However, if the alkylidene is viewed as a X_2 ligand, this mechanism requires a change of the metal formal oxidation state and is therefore unlikely to be relevant for polymerization processes involving d^0 transition-metal catalysts.

Later studies have discussed the role of α-C–H agostic interactions in the ground state and/or in the transition state to assist the olefin insertion step, favoring the stereoselective insertion of α-olefins (e.g. propylene) into the growing polymer chain (Fig. 1c) (21-26). A selection of olefin polymerization catalysts is shown in Fig. 1d (13, 27-31).

In oligomerization processes, such as the selective dimerization and trimerization of ethylene with catalysts based on early transition metals such as Ti, Ta or Cr, metallacyclopentanes and in some cases metallacycloheptanes have been proposed as key reaction intermediates (Fig. 2a) (32-44). In fact, Cp_2M(ethylene) complexes (M = Ti, Zr, and Hf) are known to react with ethylene to generate the corresponding metallacyclopentane, $Cp_2M(C_4H_8)$, in a stoichiometric manner (45-47). The industrially important ethylene dimerization catalyst that is prepared from $(BuO)_4Ti$ and $AlEt_3$ is thought to involve the corresponding putative isolobal $(BuO)_2Ti$(ethylene) and titanacyclopentane complexes (Fig. 2b) (48-49), while a catalytic trimerization is observed with isoelectronic cationic Ti species derived from $Cp(\eta^x$-$Ar)TiCl_3$ for instance (Fig. 2c) (50-52). The formation of the metallacyclopentane intermediate is often described as an oxidative coupling of two ethylene molecules because of the change of formal oxidation state from a d^2 Ti(II) olefin complex to a d^0 Ti(IV) metallacyclopentane complex. Alternatively, this step can also be viewed as a non-oxidative ethylene insertion reaction in the metallacyclopropane, similar to the elementary step involved in formation of the metallacycloheptane from the metallacyclopentane (Fig. 2a).

Recent studies on alkene and alkyne metathesis catalysts have shown that combining solid-state NMR spectroscopy and analysis of the chemical shift tensors provides information on the nature of the fron-

tier molecular orbitals and the localization of low-lying empty orbitals in transition metal complexes, giving information about the nature of the metal-carbon chemical bond and associated reactivity (53-58). We thus reasoned that a chemical shift analysis based on a combined experimental and computational approach would be a valuable tool to probe the electronic structure of reaction intermediates in polymerization and oligomerization processes and to identify key requirements that differentiate between active and inactive catalysts or between dimerization and trimerization catalysts. In this article, we show that the NMR chemical shift tensors of the α-carbon in compounds, that undergo olefin insertion and ring expansion, are diagnostic of their reactivity. They provide signatures for the presence of alkylidenic character in the metal-carbon bond, which results from the interaction of the π-donor alkyl group with an empty metal d-orbital of low energy and appropriate symmetry. This partial π-bond character is an essential ingredient for insertion and ring expansion steps found in both olefin polymerization and oligomerization processes involving group 4 metal complexes. This indicates that olefin insertion and ring expansion can be viewed as [2+2]-cycloaddition reactions, thus relating these reactions to olefin metathesis.

Results

Measurement and calculation of chemical shift tensors (CST). The following organometallic compounds are prepared and characterized by solid state NMR: the olefin polymerization precatalysts Cp_2MEtCl (M = Ti, Zr, and Hf) (59), as well as the cationic species $[Cp_2ZrMe(thf)]^+[BPh_4]^-$ (60) as a model compound for ethylene polymerization catalysts. We use 2–component DFT/ZORA calculations to analyze the shielding tensors of Cp_2MRCl (R = Et) and the cationic species Cp_2MR^+ (M = Ti, Zr, and Hf ; R = Me, Et, and Bu) as well as selected ethylene-adducts $Cp_2MR(C_2H_4)^+$, and isolable thf-adducts $Cp_2MR(thf)^+$ (Fig. 3a). For compounds with β-hydrogens, both the α-agostic and β-agostic structures are calculated (see Supporting Information for full Computational Details).

For the investigation of oligomerization processes, the relevant olefin complexes and metallacycloalkanes are calculated: $Cp_2M(C_2H_4)$, $Cp_2M(C_2H_4)_2$ and $Cp_2M(C_4H_8)$ (M = Ti, Zr, and Hf) as well as the cationic oligomerization intermediates $Cp(\eta^x\text{-Ar})Ti(C_2H_4)^+$, $Cp(\eta^x\text{-Ar})Ti(C_2H_4)_2^+$, $Cp(\eta^x\text{-Ar})Ti(C_4H_8)^+$ and $Cp(\eta^x\text{-Ar})Ti(C_6H_{12})^+$ (Fig. 3b). The solid-state NMR spectra of the model compounds $[(C_5Me_5)_2Ti(C_2H_4)]$ and $Cp_2Zr(C_4H_8)$ are also measured experimentally.

The chemical shifts (δ_{iso}, δ_{11}, δ_{22}, δ_{33}) for all analyzed Zr-based compounds related to olefin polymerization are shown in Table 1, along with selected Ti and Hf derivatives. The data for Ti-based compounds related to olefin oligomerization and selected Zr compounds are summarized in Table 2. Good agreement between calculated and experimental values is obtained, when data are available. A complete list of all calculated compounds is given in Table S1.

Even though many computational studies have been carried out on these complexes and their role in oligo- and polymerization reactions (63-79), the electronic structures and relative energies of relevant reactants, intermediates, and transition states are computed with the same method used for optimizing the geometries for NMR calculations for consistency.

Development of the CST along reaction pathways.

Olefin polymerization. This sub-section focuses on Zr-based olefin polymerization catalysts. The CST of analogous Ti- and Hf-compounds follow a similar trend, with the Ti-compounds having the most deshielded values (Fig. S1 and S2). The development of the CST during ethylene polymerization is summarized in Fig. 4a. The most significant changes of the CST are associated with the most deshielded δ_{11} component, that is oriented perpendicular to the σ_h plane for all of the aforementioned compounds.

The δ_{11} component is moderately deshielded in $Cp_2ZrEtCl$ (δ_{11} = 102 ppm). The calculations show that upon abstraction of the Cl^- ligand, Cp_2ZrEt^+ can exist both in a β-H agostic and α-H agostic structure. The β-H agostic compound is calculated to be preferred by around 4.5 kcal mol^{-1}, in agreement with previous studies (64-67). Since olefin insertion into metal-carbon bonds has been proposed to be assisted by an α-H agostic interaction, in the ground and/or the transition state (24, 26, 66-67), we calculate both the α-H and β-H agostic complexes and the associated transition states for insertion. Ethylene coordination and the transition state for insertion are more favored for the α-H agostic Cp_2ZrEt^+ (ΔG = –3.6 kcal mol^{-1} and $\Delta G^{‡}$ = 1.4 kcal mol^{-1}), relative to the β-H agostic Cp_2ZrEt^+ (ΔG = 6.0 kcal mol^{-1} and $\Delta G^{‡}$ = 9.1 kcal mol^{-1}). The more favorable calculated pathway found for the α-H agostic compound suggests that this intermediate is the reactive state of the catalyst, while the β-H agostic Cp_2ZrEt^+ complex is the resting state, which is in accordance with previous studies (66-67).
As compared to $Cp_2ZrEtCl$, the δ_{11} component of Cp_2ZrEt^+ is more deshielded in both the β-H and α-H agostic structures, but this effect is much more pronounced in the latter (Fig. 4a). Upon ethylene coordination, the development of the CST in the two structures diverges: the δ_{11} component becomes significantly more shielded in the β-H agostic structure, leading to a more isotropic CST, while the δ_{11} component becomes even more deshielded for the α-H agostic structure, generating a highly anisotropic CST. The corresponding β-H and α-H agostic butyl-complexes Cp_2ZrBu^+ show very similar tensors to those in Cp_2ZrEt^+, indicating that the foregoing analysis applies to the first and second insertion steps and likely to all stages of the polymerization process. Notably, ethylene insertion into the metal-alkyl complex leads to a migration of the alkyl chain to the adjacent site, while keeping alkylidene character on the α-carbon. This is particularly evident for the α-H agostic complex, which is consistent with polymer chain growth with alternating coordination site at each insertion step, which is of key importance to explain stereoselectivity in the polymerization process (80).

Olefin oligomerization. The development of the CST during ethylene oligomerization is illustrated in Fig. 4b for both the neutral Cp_2Ti- and the cationic $Cp(\eta^x\text{-}Ar)Ti^+$-based systems. Again, it is apparent that the most significant changes of the CST are associated with the δ_{11} component, which is oriented similarly in the studied compounds (perpendicular to the σ_h or pseudo-σ_h plane, see Fig. 4b). This component is highly deshielded for $Cp_2Ti(C_2H_4)$, which inserts an olefin with a moderate Gibbs energy of activation, forming the corresponding metallacyclopentane (ΔG = 13.4 kcal mol^{-1} for the formation of the bis-ethylene adduct and $\Delta G^{‡}$ = 8.0 kcal mol^{-1} for metallacyclopentane formation). While δ_{11} is similar for the ethylene carbon in $Cp_2Ti(C_2H_4)$ and free ethylene (Table 2), the shape of the associated tensors is different as shown by the different values of the δ_{22} component that are 41 and 124 ppm for $Cp_2Ti(C_2H_4)$ and C_2H_4, respectively. In the corresponding bis-ethylene adduct $Cp_2Ti(C_2H_4)_2$ and metallacyclopentane $Cp_2Ti(C_4H_8)$ the δ_{11} component is much more shielded, giving rise to only moderately anisotropic CSTs, which is also true for the corresponding metallacycloheptane. The latter molecule is however not detected experimentally, since no ethylene insertion is observed in $Cp_2Ti(C_4H_8)$. Similar observations are made for the corresponding Zr- and Hf-based systems (see Supporting Information, Fig. S3 and S4).
In sharp contrast to $Cp_2Ti(C_2H_4)_2$ and $Cp_2Ti(C_4H_8)$, the analogous cationic bis-ethylene complex $Cp(\eta^x\text{-}Ar)Ti(C_2H_4)_2^+$ and metallacyclopentane $Cp(\eta^x\text{-}Ar)Ti(C_4H_8)^+$, which are proposed intermediates in the ethylene trimerization process (73-76), show a large deshielding on the α-carbons, associated with a strongly deshielded δ_{11} component, giving rise to strongly anisotropic CSTs. The corresponding metallacycloheptane $Cp(\eta^x\text{-}Ar)Ti(C_6H_{12})^+$, formed after insertion of an ethylene molecule into the metal-carbon bond of $Cp(\eta^x\text{-}Ar)Ti(C_4H_8)^+$ also shows a deshielded δ_{11} component, albeit less pronounced in comparison to the metallacyclopentane $Cp(\eta^x\text{-}Ar)Ti(C_4H_8)^+$. The larger deshielding in $Cp(\eta^x\text{-}Ar)Ti(C_2H_4)_2$

and $Cp(\eta^x\text{-}Ar)Ti(C_4H_8)^+$ as compared to $Cp_2Ti(C_2H_4)_2$ and $Cp_2Ti(C_4H_8)$ corresponds to an energetically more accessible metallacyclopentane and metallacycloheptane formation in the reaction with ethylene. The calculated Gibbs energies of activation are $\Delta G^{\ddagger}$ = +5.5 and +8.0 kcal mol^{-1} for metallacyclopentane formation from $Cp(\eta^x\text{-}Ar)Ti(C_2H_4)_2^+$ and $Cp_2Ti(C_2H_4)_2$, respectively, and $\Delta G^{\ddagger}$ = +15.5 and +51.0 kcal mol^{-1} for the associated metallacycloheptane formation.

Analysis of the chemical shift tensors (CSTs).

Augmenting the NMR chemical shift tensor analysis with DFT calculations illuminates the interpretation of experimental results. This approach has recently emerged as a powerful tool for studying the electronic structure of organometallic compounds (81-108), including catalysts and catalytic reaction intermediates (53, 55-58). The approach is particularly attractive since chemical shift is a property that depends on frontier molecular orbitals, whose contributions can be analyzed through quantum chemical calculations, allowing for a detailed understanding of molecular electronic structure.

The shielding tensor σ, as calculated by computational methods, is related to the experimentally determined chemical shift tensor δ by a shift of the origin (eq. 1). The shielding σ can be decomposed into diamagnetic and paramagnetic plus spin-orbit contributions (eq. 2). For the compounds investigated in this article, the diamagnetic contributions are found to be similar for all compounds (Table S2), and spin-orbit contributions are found to be small (Table S6). The variations of the chemical shift are thus largely due to paramagnetic contributions, which also lead to the large deshielding of the δ_{11} component. The paramagnetic contributions to deshielding originate from the magnetically induced coupling of excited electronic states with the ground state, by action of the angular momentum operator $\hat{L}_i$ (i = 1-3, eq. 3). Hence, chemical shift is sensitive to the relative energy and orientation of frontier orbitals, thus establishing a link to molecular reactivity. For atomic carbon p-orbitals, deshielding by $\hat{L}_i$ arises when the vacant and occupied orbitals are oriented perpendicular to each other and to the i-axis, as schematically illustrated below for the case of ethylene.

$$\delta_{ii} = \sigma_{iso}^{ref} - \sigma_{ii} \qquad (1)$$

$$\sigma = \sigma_{dia} + \sigma_{para+SO} \qquad (2)$$

$$\sigma_{ii,para} \Leftrightarrow \frac{\langle \Psi_{vac}|\hat{L}_i|\Psi_{occ}\rangle\langle \Psi_{vac}|\hat{L}_i/r^3|\Psi_{occ}\rangle}{\Delta E_{vac-occ}} \qquad (3)$$

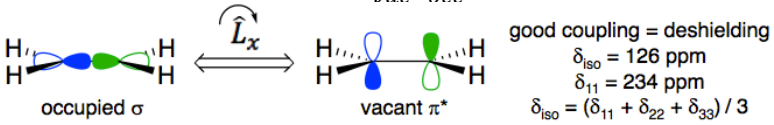

In order to understand the observed deshielding of the carbon chemical shift in the metal alkyl compounds at the frontier orbital level, the shielding tensors of representative compounds are analyzed by an orbital analysis, closely related to the Natural Chemical Shift (NCS) analysis. (83, 92, 109) We focus on the δ_{11} component, since this component has the largest influence and is mostly responsible for the observed trends (The NCS analyses for all components are given in the Supporting Information).

Olefin polymerization. The CST values given in this sub-section focus on the species derived from the Cp_2Zr fragment, but the general findings also apply to the isoelectronic Ti and Hf systems (see Supporting Information). The orbital analysis reveals that deshielding of the δ_{11} component in $Cp_2ZrEtCl$, Cp_2ZrMe^+, Cp_2ZrEt^+, $Cp_2ZrEt(C_2H_4)^+$ and Cp_2ZrBu^+ mainly arises from the contribution of the σ(M–C) bond to the paramagnetic component of δ_{11} (Fig. 5a). The contribution of σ(M–C) increases upon going from $Cp_2ZrEtCl$ to β-H agostic Cp_2ZrEt^+. This, together with a significant contribution from the $\sigma(C_\alpha–C_\beta)$ bond, results in a more strongly deshielded δ_{11} component in the latter system. In the α-H agostic analogue of Cp_2ZrEt^+ (or in Cp_2ZrMe^+), the deshielding of the δ_{11} component of the CST on the α-carbon is

significantly more pronounced. This is mostly associated with a larger contribution of the σ(M–C) orbital, combined with significant contributions arising from the σ(C_α–C_β) and the σ(C–H) bonds.
Coordination of ethylene to the β-H agostic and α-H agostic structures of Cp_2ZrEt^+ leads to distinctively different CSTs on the α-carbon in the β-H and α-H agostic structures of $Cp_2ZrEt(C_2H_4)^+$. In the case of the β-H agostic structure, the coordinated olefin leads to a significant shielding of δ_{11}, mainly due to a decreased contribution of the σ(M–C) bond to deshielding. On the other hand, coordination of ethylene to the α-H agostic analogue increases the deshielding of the α-carbon as compared to α-H agostic Cp_2ZrEt^+. This is mainly due to a strong increase of the contribution of the σ(M–C) bond to deshielding (Fig. 5a). The Cp_2ZrBu^+ compounds behave similarly to Cp_2ZrEt^+.

Olefin oligomerization. The compounds related to olefin oligomerization are analyzed, focusing on Ti-based systems due to their importance in catalysis; similar patterns are obtained for the Zr- and Hf-analogues as reported in the Supporting Information. In the Ti-compounds shown in Fig. 5b, the σ(M–C) orbital constitutes the largest contribution to the δ_{11} component. Comparing $Cp_2Ti(C_2H_4)$ and $Cp_2Ti(C_4H_8)$ reveals that the contribution to deshielding of the σ(M–C) orbital is significantly larger in the former, in accord with the overall more deshielded δ_{11} component and δ_{iso} (Table 2, Fig. 5b). While the α-carbon of $Cp_2Ti(C_4H_8)$ is not strongly deshielded, in the cationic metallacyclopentane, $Cp(\eta^x\text{-}Ar)Ti(C_4H_8)^+$, the situation is different. This cationic metallacyclopentane shows a large deshielding on one of its α-carbons, again mostly originating from the contribution of the σ(M–C) orbital. In the cationic metallacycloheptane, $Cp(\eta^x\text{-}Ar)Ti(C_6H_{12})^+$, the situation is somewhat similar, albeit δ_{11} of the α-carbon is less deshielded, due to a smaller contribution of the σ(M–C) orbital, but also the σ(C–C) and σ(C–H) orbitals (Fig. 5b).

Analysis of electronic structure based on CSTs

Olefin Polymerization. The differences in the CST values of the various compounds are mainly determined by the δ_{11} component, which has a similar orientation in all investigated molecules (Fig. 4). This component of the CST is hence a valuable reporter of the electronic structure of the various compounds. As noted in previous studies (53, 55-58), the large deshielding of δ_{11} originating from the σ(M–C) bond implies the presence of a low-lying vacant orbital, oriented perpendicular to both the σ(M–C) bond and the direction of the δ_{11} component as illustrated in Fig. 6a. This vacant orbital originates from a p-orbital on the α-carbon, interacting with a low-lying empty metal d-orbital in the approximate σ_h plane that is present in all aforementioned systems. The interaction of the metal with the α-carbon generates a low-lying vacant orbital of π*(M–C) character, which results in the large α-carbon chemical shifts and is shown for selected compounds in Fig. 6c.
Alkylidene character and thus the presence of a π*(M–C) orbital, also evidenced in a Natural Hybrid Orbital (NHO) Directionality and Bond Bending Analysis (Table S7), is present in all systems studied in this article that are prone to undergo ethylene insertion. The energetic accessibility of this orbital, and hence its ability to promote the olefin insertion process, is reflected in the magnitude of the deshielding. The large deshielding indicates a low energy of this orbital, since the paramagnetic term increases in magnitude with a smaller energy gap between the occupied σ(M–C) orbital and the empty π*(M–C) (eq. 3). This low-lying π*(M–C) orbital parallels with a low energy barrier for olefin insertion. In addition, the presence of a low-lying metal based d-orbital induces π(M–C) character (alkylidenic character) in the M–C bond. A similar π-type overlap of an empty metal d-orbital with the α-carbon has been shown to trigger olefin metathesis activity in metallacyclobutanes (56), and α-H-abstraction in bis-alkyl complexes (58).

$Cp_2ZrEtCl$ needs to lose a chloride to become an active olefin polymerization catalyst (5, 12-15, 77, 110). The calculations show that the contribution of the σ(M–C) bond to deshielding of the δ_{11} component increases upon going from neutral $Cp_2ZrEtCl$ to cationic Cp_2ZrEt^+. As noted above, this trend is particularly pronounced for Cp_2ZrMe^+ and the α-H agostic Cp_2ZrEt^+, for which ethylene insertion is more favorable, but less pronounced for Cp_2ZrEt^+ with β-H agostic interaction. Since the larger deshielding is mainly caused by the σ(M–C) orbital, this distinctive chemical shift evidences a stronger π(M–C) contribution in the more deshielded compounds. This alkylidenic character is favored by both, the positively charged and coordinatively unsaturated metal center, and is larger for the α- than for the β-H agostic structures.

The change of the values of the CST on the α-carbon of Cp_2ZrEt^+ upon ethylene coordination is as remarkable as it is surprising, since the changes are opposite in the structures with β-H and α-H agostic interactions. In the structure with a β-H agostic interaction, the resulting ethylene complex shows a rather isotropic CST on the α-carbon, mostly due to a significantly more shielded δ_{11} component. In sharp contrast, the α-carbon of α-H agostic Cp_2ZrEt^+ becomes even more deshielded upon ethylene coordination (Fig. 5a).

The deshielding of the α-carbon upon ethylene coordination to the α-H agostic structure can be understood by considering the in-phase mixing of the π^*(M–C) and the π^*(C–C) orbitals, as illustrated in Fig. 6b. This empty orbital is lower in energy than the original π^*(M–C), resulting in a smaller energy gap between σ(M–C) and π^*(M–C), hence in a larger value of the deshielding. The observed chemical shift is thus illustrative of the electron transfer from the M–C bond into the π^*(M–C)/π^*(C–C) orbital, which ultimately leads to forming and breaking of chemical bonds during the insertion process.

The fact that a similar effect on the NMR chemical shift of the α-carbon is not observed in the β-H agostic structure indicates that the agostic β-H compromises the alkylidenic character of the M–C bond. The single M–C bonds in β-H agostic and α-H agostic $Cp_2ZrEt(C_2H_4)^+$ hence differ significantly in their electronic structures, with the latter showing a much larger π(M–C) character. This correlates with the free energy of activation for the ethylene insertion process, which is significantly higher in the β-H agostic structure, while the insertion is virtually barrierless in the α-H agostic structure ($\Delta G^{\ddagger}$ = 9.1 and 1.4 kcal mol^{-1} respectively; see Fig. 4 for energy profile) indicating that the increase in alkylidene character favors insertion. In fact, the increased π-character in α-H agostic $Cp_2ZrEt(C_2H_4)^+$ is also reflected in the calculated $M–C_\alpha$ distance (2.23 Å vs. 2.29 Å in the α-H vs. β-H agostic structure, respectively). The apparent paradox is that the shorter α-H agostic M–C bond is found to be more reactive towards olefin insertion..

The Cp_2ZrBu^+ species generated upon insertion displays a CST for the α-carbon similar to Cp_2ZrEt^+, both for the β-H-agostic and α-H-agostic form, indicating that the foregoing analysis also applies to the subsequent ethylene insertions during polymer chain growth.

Olefin Oligomerization. We performed a similar analysis on the ethylene complex $Cp_2Ti(C_2H_4)$. In free ethylene, the deshielding mostly arises from the magnetically induced coupling of the σ(C–C) orbital to the vacant π^*(C–C) orbital (Fig. 7a, eq. 3). In the ethylene complex $Cp_2Ti(C_2H_4)$, the largest part of the deshielding arises from a coupling of the occupied σ(M–C) orbital with the vacant π^*(M–C) orbital (Fig. 7b). This situation resembles what is observed in the cationic metal alkyl complexes, e.g. $Cp_2M–R^+$ (Fig. 6a), and is a signature of the reactivity of the M–C bond towards olefin insertion and hence ring expansion to yield a metallacyclopentane.

In the corresponding metallacyclopentane $Cp_2Ti(C_4H_8)$, the α-carbons are significantly less deshielded, mainly due to a smaller deshielding of the δ_{11} components. According to the NCS analysis, this is caused by a significantly decreased contribution of the σ(M–C) bond to δ_{11} (Fig. 5b). This indicates that

the M–C bonds of $Cp_2Ti(C_4H_8)$ contain less π-(alkylidenic)-character. In sharp contrast, the cationic analogue $Cp(\eta^x\text{-}Ar)Ti(C_4H_8)^+$ retains a large deshielding on one of the α-carbons (δ_{iso} = 122 ppm and δ_{11} = 235 ppm). Again the largest contribution to δ_{11} arises from the σ(M–C) bond, indicating that $Cp(\eta^x\text{-}Ar)Ti(C_4H_8)^+$ retains a significant alkylidenic character, and is thus prone to further ethylene insertion (Fig. 5b). The resulting metallacycloheptane $Cp(\eta^x\text{-}Ar)Ti(C_6H_{12})^+$ shows slightly less deshielding (δ_{iso} = 115 ppm, δ_{11} = 200 ppm). This observation correlates with the Gibbs energy of activation (and corresponding reaction free energies) for the metallacycloheptane formation from $Cp_2Ti(C_4H_8)$ and $Cp(\eta^x\text{-}Ar)Ti(C_4H_8)$ which are found to be at 51.0 kcal mol^{-1} (-4.1 kcal mol^{-1}) and 15.5 kcal mol^{-1} (-25.4 kcal mol^{-1}), respectively (see Fig. 4b for Gibbs energy profile). Also in these systems related to ethylene oligomerization the NHO Directionality and Bond Bending Analysis indicates the presence of π-character in the M–C bonds that are prone to insert olefins and feature a deshielded α-carbon (Table S7).

Discussion

All calculations and experimental evidence from the literature agree that insertion of ethylene into a metal-carbon bond of a low-electron count transition metal, such as a cationic species like $Cp_2Ti\text{–}CH_2R^+$, is an exoergic reaction that proceeds with a small Gibbs activation energy. The net reaction is classified as a [2σ+2π] cycloaddition which would be symmetry forbidden in organic transformations, but can occur in the presence of transition metals. It is thought that the activation energy is influenced by a distortion of [M]–CH_2R in the ground and/or the transition state, resulting in a short $M^{\cdots}H_\alpha$ contact distance in the structure of the catalyst (26). The resulting shortened metal-carbon bond distance is often associated with an acute [M–C–H] angle and an increase in the C–H distance; this distortion is referred to as an α-H agostic interaction. The α-H agostic interaction is attributed in part to the donation of electron density from the α-C–H bond to a vacant metal orbital (21, 111-113), resulting in a lowering of the $^1J_{C\text{-}H}$ coupling constant, due to the increased p-character in the C_α–H bond.

In this article, the measured solid-state NMR tensors show that the α-carbon is highly anisotropic, unexpected for a σ-alkyl. Computations indicate the specific orientation of the anisotropic chemical shift tensor, with the most deshielded component (δ_{11}) oriented perpendicular to the symmetry or pseudo symmetry plane of the molecules (Fig. 4). NCS analysis shows that the deshielding originates from the presence of a low-lying empty metal d-orbital that interacts in a π-fashion with a filled carbon p-orbital, perpendicular to the M–C bond that is also involved in the C–H bond. Therefore, the α-C–H interaction, referred to as an agostic C–H bond, is a manifestation of the π-donation of the alkyl ligand to the electron-deficient metal center. This gives some alkylidene character to the single M–C bond and results in a shortening of the M–C distance, as proposed in one of the initial discussions of the α-C–H agostic interaction (111). A corollary is that the alkylidenic character is responsible for the geometric distortion, observed in an α-C–H agostic interaction.

The CST hence probes the frontier molecular orbitals that participate in the insertion step, *thus correlating chemical shift, in particular δ_{11}, to reactivity*. Olefin insertion is favored for metal alkyl compounds with alkylidene character, reminiscent of the reaction of an olefin with metal alkylidenes in the olefin metathesis reaction (Fig. 8). In this analogy, the difference between olefin metathesis and olefin insertion lies only in the degree of alkylidenic character in the M–C bond since in both cases an olefin reacts with a metal-carbon bond bearing π-bond character. In the case of olefin metathesis, there is a formal π(M=C) bond in the alkylidene that enables the formation of a metallacyclobutane intermediate in the [2+2] cycloaddition reaction. In an olefin insertion process, the M–C bond only carries partial π-character, resulting in the formation of a homologous metal-alkyl product rather than a metallacyclobutane product. The foregoing analogy demonstrates the complementarity between the Cossee-Arlman and the Green-Rooney mechanisms (Fig. 1); the Cossee-Arlman mechanism suggests that the

olefin insertion takes place at a metal–alkyl complex with a vacant coordination site while in the Green-Rooney mechanism the olefin is activated by the metal alkylidene. Hence, the difference between the Cossee-Arlman and the Green-Rooney mechanism consists merely in the extent of π(M–C) character in the M–C bond.

Based on the foregoing analysis, the role of charge in olefin insertion is delineated since a positive charge on the metal alkyl compound lowers the energy of the d-orbitals, bringing them closer in energy to the filled ligand orbitals, allowing for a stronger π(M–C) bonding interaction and the lower activation energies for olefin insertion.

Similarly, the observed chemical shift tensors account for the reactivity of $(BuO)_2Ti$ systems (studied in the isolobal Cp_2M compounds) towards ethylene. The ethylene adduct $Cp_2Ti(C_2H_4)$ shows significant alkylidenic character and is prone to insert an additional molecule of ethylene. However, the M–C bond of the resulting metallacyclopentane does not show significant alkylidenic character; accordingly, it is not reactive towards olefin insertion and does not undergo further ring expansion. Instead, rather stable metallacyclopentanes or β-H abstraction processes are observed, generating 1-butene. In contrast, the metallacyclopentane in the cationic $Cp(\eta^x\text{-Ar})Ti^+$ system retains a significant alkylidenic character on one α-carbon, as evidenced by a large deshielding. This also accounts for the shorter calculated M–C bond distance (2.025 Å in $Cp(\eta^x\text{-Ar})Ti(C_4H_8)^+$ vs. 2.164 Å in $Cp_2Ti(C_4H_8)$). Hence, for the cationic species, further reactivity towards ethylene insertion is expected and observed. In the resulting metallacycloheptane, the α-carbon is slightly less deshielded (δ_{11} decreases by 35 ppm, the contribution of σ(M–C) by 11 ppm). This indicates a slightly decreased alkylidenic character of the M–C bond, consistent with the slightly higher transition state energy for ethylene insertion into $Cp(\eta^x\text{-Ar})Ti(C_6H_{12})^+$ vs. $Cp(\eta^x\text{-Ar})Ti(C_4H_8)^+$ (17.2 vs. 15.5 kcal mol^{-1}). Combined with the rather low free energy of activation (14.0 kcal mol^{-1}) for β-H abstraction at the metallacycloheptane $Cp(\eta^x\text{-Ar})Ti(C_6H_{12})^+$, this explains the preferred formation of 1-hexene, over further ring expansion and formation of 1-octene and higher oligomers.

The analysis of the α-carbon CST values reveals some striking but informative differences between β-H and α-H agostic interactions. Agostic interactions are traditionally described as 3-center-2-electron interactions between a C–H bond and a metal site (7-8, 21, 113). Hence, in these structures, the C–H bond is a 2-electron ligand interacting with the metal. This view is in line with the CST analysis for the β-H agostic structures. The β-C–H bond interacts with a low-lying metal orbital, thus raising this orbital's energy and decreasing its ability to develop a π-interaction with the α-carbon, hence the more shielded α-carbon chemical shift and lower reactivity. In an α-H agostic structure, the situation is markedly different. The small $M–C_\alpha–H$ angle is a reporter of a p-orbital on the α-carbon interacting with a low-lying metal d-orbital. Hence, this type of structure evidences alkylidene character in the M–C bond, associated with higher reactivity. While the β-H agostic interaction leads to a stabilization of a metal-alkyl species and disfavors olefin insertion, the α-H agostic interaction provides π-character to the M–C bond and makes it reactive towards olefin insertion. β-H and α-H interactions are phenomenologically similar but they have a fundamentally different origin.

Epilogue

The detailed analysis of chemical shifts, by determining chemical shift tensors using solid-state NMR augmented with computational analysis, defines the nature of the frontier molecular orbitals. Since frontier molecular orbitals are the active orbitals that are involved in making and breaking chemical bonds, the anisotropy of the NMR chemical shifts of carbon nuclei (bound to a metal) map their electronic and structural changes along the reaction coordinate. This article focuses on a selected subset of catalysts used in olefin oligo- and polymerization processes and connects them with the olefin metathesis catalysts by sharing a similar [2+2]-cycloaddition step, specifically coined as insertion, that is for-

bidden in the absence of catalysts. The catalysts for these related processes – oligomerization, polymerization, and metathesis – all fulfill the same condition: they have two low-lying empty orbitals centered at the metal of appropriate topology to engage in the reaction: one to coordinate the olefin and one to install a π-character in the metal-carbon bond to facilitate olefin insertion. Fig. 9 highlights the similarity of the topology between metal alkylidene and alkyl compounds, which differ merely in the degree, but not in the nature of π-bonding. Hence, while olefin metathesis proceeds via a formal [2+2] cycloaddition, olefin insertion can be considered in a similar manner, since the two reactions are isolobal (56). It therefore follows, not surprisingly, that d^0 Cp_2M fragments are common to both polymerization and olefin metathesis catalysts and that d^0 $X_2M(=NR)$ fragments are found in oligomerization and metathesis catalysts.

The ^{13}C NMR chemical shift, and most notably δ_{11}, is directly linked to the low activation barrier of olefin insertion, since both result from the same low-lying empty orbital of π^*(M–C) character. Accordingly, it is a descriptor that predicts the reactivity of d^0 transition-metal alkyl compounds in olefin oligomerization and polymerization processes. While it does not allow discriminating highly efficient from average catalysts due to the complexity of catalytic processes, chemical shift, and more precicesly the chemical shift tensor, provides a descriptor and thereby a guideline to design potentially efficient catalysts.

References

1. Delferro M, Marks TJ (2011) Multinuclear olefin polymerization catalysts. *Chem Rev* 111:2450-2485.
2. McInnis JP, Delferro M, Marks TJ (2014) Multinuclear group 4 catalysis: Olefin polymerization pathways modified by strong metal–metal cooperative effects. *Acc Chem Res* 47:2545-2557.
3. Baier MC, Zuideveld MA, Mecking S (2014) Post-metallocenes in the industrial production of polyolefins. *Angew Chem Int Ed* 53:9722-9744.
4. Small BL (2015) Discovery and development of pyridine-bis(imine) and related catalysts for olefin polymerization and oligomerization. *Acc Chem Res* 48:2599-2611.
5. Klosin J, Fontaine PP, Figueroa R (2015) Development of group IV molecular catalysts for high temperature ethylene-α-olefin copolymerization reactions. *Acc Chem Res* 48:2004-2016.
6. Arpe H-J *Industrial Organic Chemistry*. 5 ed.; Wiley-VCH: Weinheim, 2010.
7. Hartwig J *Organotransition Metal Chemistry: From Bonding to Catalysis*. University Science Books: Sausalito, 2010.
8. Crabtree RH *The Organometallic Chemistry of the Transition Metals*. 6 ed.; Wiley: Hoboken, 2014.
9. Cossee P (1964) Ziegler-Natta catalysis I. Mechanism of polymerization of α-olefins with Ziegler-Natta catalysts. *J Catal* 3:80-88.
10. Arlman EJ (1964) Ziegler-Natta catalysis II. Surface structure of layer-lattice transition metal chlorides. *J Catal* 3:89-98.
11. Arlman EJ, Cossee P (1964) Ziegler-Natta catalysis III. Stereospecific polymerization of propene with the catalyst system $TiCl_3$-$AlEt_3$. *J Catal* 3:99-104.
12. Dyachkovskii FS, Shilova AK, Shilov AE (1967) The role of free ions in reactions of olefins with soluble complex catalysts. *J Polym Sci C Polym Symp* 16:2333-2339.
13. McKnight AL, Waymouth RM (1998) Group 4 ansa-cyclopentadienyl-amido catalysts for olefin polymerization. *Chem Rev* 98:2587-2598.
14. Chen EY-X, Marks TJ (2000) Cocatalysts for metal-catalyzed olefin polymerization: Activators, activation processes, and structure−activity relationships. *Chem Rev* 100:1391-1434.
15. Erker G (2005) Tris(pentafluorophenyl)borane: a special boron Lewis acid for special reactions. *Dalton Trans* 0:1883-1890.
16. Bochmann M (2010) The chemistry of catalyst activation: The case of group 4 polymerization catalysts. *Organometallics* 29:4711-4740.
17. Hart DW, Schwartz J (1974) Hydrozirconation. Organic synthesis via organozirconium intermediates. Synthesis and rearrangement of alkylzirconium(IV) complexes and their reaction with electrophiles. *J Am Chem Soc* 96:8115-8116.
18. Green MLH (1978) Studies on synthesis, mechanism and reactivity of some organo-molybdenum and -tungsten compounds. *Pure Appl Chem* 50:27-35.
19. Ivin KJ, Rooney JJ, Stewart CD, Green MLH, Mahtab R (1978) Mechanism for the stereospecific polymerization of olefins by Ziegler-Natta catalysts. *J Chem Soc, Chem Commun* 0:604-606.
20. Turner HW, Schrock RR, Fellmann JD, Holmes SJ (1983) Alkylidene hydride complexes of tantalum and the polymerization of ethylene by diiodotris(trimethylphosphine)hydroneopentylidenetantalum [$Ta(CHCMe_3)(H)(PMe_3)_3I_2$]. *J Am Chem Soc* 105:4942-4950.
21. Brookhart M, Green MLH (1983) Carbon-hydrogen-transition metal bonds. *J Organomet Chem* 250:395-408.

22. Krauledat H, Brintzinger H-H (1990) Isotope effects associated with α-olefin insertion in zirconocene-based polymerisation catalysts: Evidence for an α-agostic transition state. *Angew Chem Int Ed Engl* 29:1412-1413.
23. Röll W, Brintzinger H-H, Rieger B, Zolk R (1990) Stereo- and regioselectivity of chiral, alkyl-substituted ansa-zirconocene catalysts in methylalumoxane-activated propene polymerization. *Angew Chem Int Ed Engl* 29:279-280.
24. Piers WE, Bercaw JE (1990) α Agostic assistance in Ziegler-Natta polymerization of olefins. Deuterium isotopic perturbation of stereochemistry indicating coordination of an α carbon-hydrogen bond in chain propagation. *J Am Chem Soc* 112:9406-9407.
25. Cotter WD, Bercaw JE (1991) Investigations of the magnitude of steric and α deuterium kinetic isotope effects in a carbon-carbon bond-forming reaction of a permethylscandocene complex. *J Organomet Chem* 417:C1-C6.
26. Grubbs RH, Coates GW (1996) α-Agostic Interactions and Olefin Insertion in Metallocene Polymerization Catalysts. *Acc Chem Res* 29:85-93.
27. Sinn H, Kaminsky W, Vollmer HJ, Woldt R (1980) "Living Polymers" on polymerization with extremely productive Ziegler catalysts. *Angew Chem Int Ed Engl* 19:390-392.
28. Chen Y-X, Marks TJ (1997) "Constrained Geometry" dialkyl catalysts. Efficient syntheses, C−H bond activation chemistry, monomer−dimer equilibration, and α-olefin polymerization catalysis. *Organometallics* 16:3649-3657.
29. Tshuva EY, Goldberg I, Kol M (2000) Isospecific living polymerization of 1-hexene by a readily available nonmetallocene C_2-symmetrical zirconium catalyst. *J Am Chem Soc* 122:10706-10707.
30. Boussie TR, Diamond GM, Goh C, Hall KA, LaPointe AM, Leclerc MK, Murphy V, Shoemaker JAW, Turner H, Rosen RK, Stevens JC, Alfano F, Busico V, Cipullo R, Talarico G (2006) Nonconventional catalysts for isotactic propene polymerization in solution developed by using high-throughput-screening technologies. *Angew Chem Int Ed* 45:3278-3283.
31. Collins RA, Russell AF, Mountford P (2015) Group 4 metal complexes for homogeneous olefin polymerisation: a short tutorial review. *Appl Petrochem Res* 5:153-171.
32. Briggs JR 1987 US4668838.
33. Andes C, Harkins SB, Murtuza S, Oyler K, Sen A (2001) New tantalum-based catalyst system for the selective trimerization of ethene to 1-hexene. *J Am Chem Soc* 123:7423-7424.
34. Yu Z-X, Houk KN (2003) Why trimerization? Computational elucidation of the origin of selective trimerization of ethene catalyzed by $[TaCl_3(CH_3)_2]$ and an agostic-assisted hydride transfer mechanism. *Angew Chem Int Ed* 42:808-811.
35. McGuinness DS, Wasserscheid P, Keim W, Morgan D, Dixon JT, Bollmann A, Maumela H, Hess F, Englert U (2003) First Cr(III)−SNS complexes and their use as highly efficient catalysts for the trimerization of ethylene to 1-hexene. *J Am Chem Soc* 125:5272-5273.
36. McGuinness DS, Wasserscheid P, Keim W, Hu C, Englert U, Dixon JT, Grove C (2003) Novel Cr-PNP complexes as catalysts for the trimerisation of ethylene. *Chem Commun* 0:334-335.
37. Dixon JT, Green MJ, Hess FM, Morgan DH (2004) Advances in selective ethylene trimerisation – a critical overview. *J Organomet Chem* 689:3641-3668.
38. Agapie T, Schofer SJ, Labinger JA, Bercaw JE (2004) Mechanistic studies of the ethylene trimerization reaction with chromium−diphosphine catalysts: Experimental evidence for a mechanism involving metallacyclic intermediates. *J Am Chem Soc* 126:1304-1305.
39. Blann K, Bollmann A, Dixon JT, Neveling A, Morgan DH, Maumela H, Killian E, Hess M, Otto S, Overett MJ 2004 WO2004056477

40. Blann K, Bollmann A, Dixon JT, Hess FM, Killian E, Maumela H, Morgan DH, Neveling A, Otto S, Overett MJ (2005) Highly selective chromium-based ethylene trimerisation catalysts with bulky diphosphinoamine ligands. *Chem Commun* 0:620-621.
41. Forestière A, Olivier-Bourbigou H, Saussine L (2009) Oligomerization of monoolefins by homogeneous catalysts. *Oil & Gas Science and Technology - Rev. IFP* 64:649-667.
42. Arteaga-Müller R, Tsurugi H, Saito T, Yanagawa M, Oda S, Mashima K (2009) New tantalum ligand-free catalyst system for highly selective trimerization of ethylene affording 1-hexene: New evidence of a metallacycle mechanism. *J Am Chem Soc* 131:5370-5371.
43. McGuinness DS (2011) Olefin oligomerization via metallacycles: Dimerization, trimerization, tetramerization, and beyond. *Chem Rev* 111:2321-2341.
44. Chen Y, Callens E, Abou-Hamad E, Merle N, White AJP, Taoufik M, Copéret C, Le Roux E, Basset J-M (2012) [(≡SiO)$Ta^{V}Cl_2Me_2$]: A well-defined silica-supported tantalum(V) surface complex as catalyst precursor for the selective cocatalyst-free trimerization of ethylene. *Angew Chem Int Ed* 51:11886-11889.
45. Negishi E-I, Takahashi T (1994) Patterns of stoichiometric and catalytic reactions of organozirconium and related complexes of synthetic interest. *Acc Chem Res* 27:124-130.
46. Negishi E, Choueiry D, Nguyen TB, Swanson DR, Suzuki N, Takahashi T (1994) Nonconcerted paths for reactions of alkene-zirconocene complexes. *J Am Chem Soc* 116:9751-9752.
47. Tamotsu T, Reinald F, Zhenfeng X, Kiyohiko N (1996) Isolation and characterization of zirconacyclopentane. *Chem Lett* 25:357-358.
48. Chauvin Y, Commereuc D, Glaize Y 1986 EP0200654.
49. Chauvin Y (2006) Olefin metathesis: The early days (Nobel Lecture). *Angew Chem Int Ed* 45:3740-3747.
50. Deckers PJW, Hessen B, Teuben JH (2001) Switching a catalyst system from ethene polymerization to ethene trimerization with a hemilabile ancillary ligand. *Angew Chem Int Ed* 40:2516-2519.
51. Deckers PJW, Hessen B, Teuben JH (2002) Catalytic trimerization of ethene with highly active cyclopentadienyl−arene titanium catalysts. *Organometallics* 21:5122-5135.
52. Otten E, Batinas AA, Meetsma A, Hessen B (2009) Versatile coordination of cyclopentadienyl-arene ligands and its role in titanium-catalyzed ethylene trimerization. *J Am Chem Soc* 131:5298-5312.
53. Halbert S, Copéret C, Raynaud C, Eisenstein O (2016) Elucidating the link between NMR chemical shifts and electronic structure in d^0 olefin metathesis catalysts. *J Am Chem Soc* 138:2261-2272.
54. Copéret C, Liao W-C, Gordon CP, Ong T-C (2017) Active sites in supported single-site catalysts: An NMR perspective. *J Am Chem Soc* 139:10588-10596.
55. Yamamoto K, Gordon CP, Liao W-C, Copéret C, Raynaud C, Eisenstein O (2017) Orbital analysis of carbon-13 chemical shift tensors reveals patterns to distinguish Fischer and Schrock carbenes. *Angew Chem Int Ed* 56:10127-10131.
56. Gordon CP, Yamamoto K, Liao W-C, Allouche F, Andersen RA, Copéret C, Raynaud C, Eisenstein O (2017) Metathesis activity encoded in the metallacyclobutane carbon-13 NMR chemical shift tensors. *ACS Cent Sci* 3:759-768.
57. Estes DP, Gordon CP, Fedorov A, Liao WC, Ehrhorn H, Bittner C, Zier ML, Bockfeld D, Chan KW, Eisenstein O, Raynaud C, Tamm M, Coperet C (2017) Molecular and silica-supported molybdenum alkyne metathesis catalysts: Influence of electronics and dynamics on activity revealed by kinetics, solid-state NMR, and chemical shift analysis. *J Am Chem Soc* 139:17597-17607.

58. Gordon CP, Yamamoto K, Searles K, Shirase S, Andersen RA, Eisenstein O, Copéret C (2018) Metal alkyls programmed to generate metal alkylidenes by α-H abstraction: prognosis from NMR chemical shift. *Chem Sci* 9:1912-19*18*
59. Long WP, Breslow DS (1960) Polymerization of ethylene with bis-(cyclopentadienyl)-titanium dichloride and diethylaluminum chloride. *J Am Chem Soc* 82:1953-1957.
60. Jordan RF, Bajgur CS, Dasher WE, Rheingold AL (1987) Hydrogenation of cationic dicyclopentadienylzirconium(IV) alkyl complexes. Characterization of cationic zirconium(IV) hydrides. *Organometallics* 6:1041-1051.
61. J Jordan RF, LaPointe RE, Bradley PK, Baenziger N (1989) Synthesis and chemistry of cationic alkyl, alkenyl, and allyl complexes derived from the soluble, cationic hydride $(C_5H_4Me)_2Zr(H)(THF)^+$. *Organometallics* 8:2892-2903.
62. Zilm KW, Conlin RT, Grant DM, Michl J (1980) Low-temperature carbon-13 magnetic resonance of solids. 1. Alkenes and cycloalkenes. *J Am Chem Soc* 102:6672-6676.
63. Kawamura-Kuribayashi H, Koga N, Morokuma K (1992) An ab initio MO study on ethylene and propylene insertion into the titanium-methyl bond in $CH_3TiCl_2^+$ as a model of homogeneous olefin polymerization. *J Am Chem Soc* 114:2359-2366.
64. Woo TK, Fan L, Ziegler T (1994) A density functional study of chain growing and chain terminating steps in olefin polymerization by metallocene and constrained geometry catalysts. *Organometallics* 13:2252-2261.
65. Lohrenz JCW, Woo TK, Ziegler T (1995) A density functional study on the origin of the propagation barrier in the homogeneous ethylene polymerization with Kaminsky-type catalysts. *J Am Chem Soc* 117:12793-12800.
66. Margl P, Lohrenz JCW, Ziegler T, Blöchl PE (1996) A dynamical density functional study on the reaction of ethylene with $Cp_2Zr(C_2H_5)^+$. *J Am Chem Soc* 118:4434-4441.
67. Margl P, Deng L, Ziegler T (1998) A unified view of ethylene polymerization by d^0 and d^0f^n transition metals. Part 2: Chain propagation. *J Am Chem Soc* 120:5517-5525.
68. Karl J, Dahlmann M, Erker G, Bergander K (1998) Arriving at an experimental estimate of the intrinsic activation barrier of olefin insertion into the Zr−C bond of an active metallocene Ziegler catalyst. *J Am Chem Soc* 120:5643-5652.
69. Schmid R, Ziegler T (2000) Polymerization catalysts with d^n electrons (n = 1−4): A theoretical study. *Organometallics* 19:2756-2765.
70. Rappé AK, Skiff WM, Casewit CJ (2000) Modeling metal-catalyzed olefin polymerization. *Chem Rev* 100:1435-1456.
71. Lanza G, Fragalà IL, Marks TJ (2001) Metal and ancillary ligand structural effects on ethylene insertion processes at cationic group 4 centers. A systematic, comparative quantum chemical investigation at various ab initio levels. *Organometallics* 20:4006-4017.
72. Tobisch S, Ziegler T (2003) Catalytic linear oligomerization of ethylene to higher α-olefins: Insight into the origin of the selective generation of 1-hexene promoted by a cationic cyclopentadienyl-arene titanium active catalyst. *Organometallics* 22:5392-5405.
73. Blok ANJ, Budzelaar PHM, Gal AW (2003) Mechanism of ethene trimerization at an ansa-(arene)(cyclopentadienyl) titanium fragment. *Organometallics* 22:2564-2570.
74. de Bruin TJM, Magna L, Raybaud P, Toulhoat H (2003) Hemilabile ligand induced selectivity: a DFT study on ethylene trimerization catalyzed by titanium complexes. *Organometallics* 22:3404-3413.
75. Tobisch S, Ziegler T (2004) Catalytic oligomerization of ethylene to higher linear α-olefins promoted by cationic group 4 cyclopentadienyl-arene active catalysts: A DFT investigation

exploring the influence of electronic factors on the catalytic properties by modification of the hemilabile arene functionality. *Organometallics* 23:4077-4088.

76. de Bruin T, Raybaud P, Toulhoat H (2008) A DFT chemical descriptor to predict the selectivity in α-olefins in the catalytic metallacyclic oligomerization reaction of ethylene according to the (hemi)labile ligand coordinating to titanium. *Organometallics 2*7:4864-4872.
77. Sauriol F, Wong E, Leung AMH, Donaghue IE, Baird MC, Wondimagegn T, Ziegler T (2009) Structures and properties of nonchelated, d^0 alkyl alkene complexes of the type $[Cp_2ZrMe(alkene)]^+$: Elusive intermediates during Ziegler–Natta polymerizations of alkenes. *Angew Chem Int Ed* 48:3342-3345.
78. Laine A, Linnolahti M, Pakkanen TA, Severn JR, Kokko E, Pakkanen A (2010) Comparative theoretical study on homopolymerization of α-olefins by bis(cyclopentadienyl) zirconocene and hafnocene: Elemental propagation and termination reactions between monomers and metals. *Organometallics* 29:1541-1550.
79. Dunlop-Brière AF, Budzelaar PHM, Baird MC (2012) α- and β-agostic alkyl–titanocene complexes. *Organometallics* 31:1591-1594.
80. Leclerc MK, Brintzinger HH (1995) ansa-Metallocene derivatives. 31. Origins of stereoselectivity and stereoerror formation in ansa-zirconocene-catalyzed isotactic propene polymerization. A deuterium labeling study. *J Am Chem Soc* 117:1651-1652.
81. Ruiz-Morales Y, Schreckenbach G, Ziegler T (1996) Theoretical study of ^{13}C and ^{17}O NMR shielding tensors in transition metal carbonyls based on density functional theory and gauge-including atomic orbitals. *J Phys Chem* 100:3359-3367.
82. Wu G, Rovnyak D, Johnson MJA, Zanetti NC, Musaev DG, Morokuma K, Schrock RR, Griffin RG, Cummins CC (1996) Unusual ^{31}P chemical shielding tensors in terminal phosphido complexes containing a phosphorus−metal triple bond. *J Am Chem Soc* 118:10654-10655.
83. Bohmann JA, Weinhold F, Farrar TC (1997) Natural chemical shielding analysis of nuclear magnetic resonance shielding tensors from gauge-including atomic orbital calculations. *J Chem Phys* 107:1173-1184.
84. Salzmann R, Kaupp M, McMahon MT, Oldfield E (1998) Solid-state nuclear magnetic resonance spectroscopic and quantum chemical investigation of ^{13}C and ^{17}O chemical shift tensors, ^{17}O nuclear quadrupole coupling tensors, and bonding in transition-metal carbonyl complexes and clusters. *J Am Chem Soc* 120:4771-4783.
85. Wiberg KB, Hammer JD, Zilm KW, Cheeseman JR, Keith TA (1998) NMR chemical shifts. 1. The role of relative atomic orbital phase in determining the sign of the paramagnetic terms: ClF, CH_3F, $CH_3NH_3^+$, FNH_3^+, and HC∶CF. *J Phys Chem A* 102:8766-8773.
86. Wiberg KB, Hammer JD, Zilm KW, Cheeseman JR (1999) NMR chemical shifts. 3. A comparison of acetylene, allene, and the higher cumulenes. *J Org Chem* 64:6394-6400.
87. Greco JB, Peters JC, Baker TA, Davis WM, Cummins CC, Wu G (2001) Atomic carbon as a terminal ligand: Studies of a carbidomolybdenum anion featuring solid-state ^{13}C NMR data and proton-transfer self-exchange kinetics. *J Am Chem Soc* 123:5003-5013.
88. Auer D, Strohmann C, Arbuznikov AV, Kaupp M (2003) Understanding substituent effects on ^{29}Si chemical shifts and bonding in disilenes. A quantum chemical analysis. *Organometallics* 22:2442-2449.
89. Sceats EL, Figueroa JS, Cummins CC, Loening NM, Van der Wel P, Griffin RG (2004) Complexes obtained by electrophilic attack on a dinitrogen-derived terminal molybdenum nitride: electronic structure analysis by solid state CP/MAS ^{15}N NMR in combination with DFT calculations. *Polyhedron* 23:2751-2768.

90. Auer D, Kaupp M, Strohmann C (2004) “Unexpected” ^{29}Si NMR chemical shifts in heteroatom-substituted silyllithium compounds: A quantum-chemical analysis. *Organometallics* 23:3647-3655.
91. Auer D, Kaupp M, Strohmann C (2005) Understanding substituent effects on ^{29}Si chemical shifts and bonding in disilynes. A quantum-chemical analysis. *Organometallics* 24:6331-6337.
92. Autschbach J (2008) Analyzing NMR shielding tensors calculated with two-component relativistic methods using spin-free localized molecular orbitals. *J Chem Phys* 128:164112.
93. Autschbach J, Zheng S (2008) Analyzing Pt chemical shifts calculated from relativistic density functional theory using localized orbitals: The role of Pt 5d lone pairs. *Magn Reson Chem* 46:S45-S55.
94. Rossini AJ, Mills RW, Briscoe GA, Norton EL, Geier SJ, Hung I, Zheng S, Autschbach J, Schurko RW (2009) Solid-state chlorine NMR of group IV transition metal organometallic complexes. *J Am Chem Soc* 131:3317-3330.
95. Epping JD, Yao S, Karni M, Apeloig Y, Driess M (2010) Si═X Multiple bonding with four-coordinate silicon? Insights into the nature of the Si═O and Si═S double bonds in stable silanoic esters and related thioesters: A combined NMR spectroscopic and computational study. *J Am Chem Soc* 132:5443-5455.
96. Standara S, Bouzkova K, Straka M, Zacharova Z, Hocek M, Marek J, Marek R (2011) Interpretation of substituent effects on ^{13}C and ^{15}N NMR chemical shifts in 6-substituted purines. *Phys Chem Chem Phys* 13:15854-15864.
97. Aquino F, Pritchard B, Autschbach J (2012) Scalar relativistic computations and localized orbital analyses of nuclear hyperfine coupling and paramagnetic NMR chemical shifts. *J Chem Theory Comput* 8:598-609.
98. Zhu J, Kurahashi T, Fujii H, Wu G (2012) Solid-state ^{17}O NMR and computational studies of terminal transition metal oxo compounds. *Chem Sci* 3:391-397.
99. Gessner VH, Meier F, Uhrich D, Kaupp M (2013) Synthesis and bonding in carbene complexes of an unsymmetrical dilithio methandiide: A combined experimental and theoretical study. *Chem Eur J* 19:16729-16739.
100. Toušek J, Straka M, Sklenář V, Marek R (2013) Origin of the conformational modulation of the ^{13}C NMR chemical shift of methoxy groups in aromatic natural compounds. *J Phys Chem A.* 117:661-669.
101. Pascual-Borras M, Lopez X, Rodriguez-Fortea A, Errington RJ, Poblet JM (2014) 17O NMR chemical shifts in oxometalates: from the simplest monometallic species to mixed-metal polyoxometalates. *Chem Sci* 5:2031-2042.
102. Vummaleti SVC, Nelson DJ, Poater A, Gomez-Suarez A, Cordes DB, Slawin AMZ, Nolan SP, Cavallo L (2015) What can NMR spectroscopy of selenoureas and phosphinidenes teach us about the π-accepting abilities of N-heterocyclic carbenes? *Chem Sci* 6:1895-1904.
103. Pascual-Borras M, Lopez X, Poblet JM (2015) Accurate calculation of ^{31}P NMR chemical shifts in polyoxometalates. *Phys Chem Chem Phys* 17:8723-8731.
104. Greif AH, Hrobarik P, Kaupp M (2017) Insights into trans-ligand and spin-orbit effects on electronic structure and ligand NMR shifts in transition-metal complexes. *Chem Eur J* 23:9790-9803.
105. Novotný J, Vicha J, Bora PL, Repisky M, Straka M, Komorovsky S, Marek R (2017) Linking the character of the metal-ligand bond to the ligand NMR shielding in transition-metal complexes: NMR contributions from spin-orbit coupling. *J Chem Theory Comput* 13:3586-3601.

106. Marchione D, Izquierdo MA, Bistoni G, Havenith RWA, Macchioni A, Zuccaccia D, Tarantelli F, Belpassi L (2017) ^{13}C NMR spectroscopy of N-heterocyclic carbenes can selectively probe σ donation in gold(I) complexes. *Chem Eur J* 23:2722-2728.
107. Lam E, Comas-Vives A, Copéret C (2017) Role of coordination number, geometry, and local disorder on ^{27}Al NMR chemical shifts and quadrupolar coupling constants: Case study with aluminosilicates. *J Phys Chem C* 121:19946-19957.
108. Engl PS, Santiago CB, Gordon CP, Liao W-C, Fedorov A, Copéret C, Sigman MS, Togni A (2017) Exploiting and understanding the selectivity of Ru-N-heterocyclic carbene metathesis catalysts for the ethenolysis of cyclic olefins to α,ω-dienes. *J Am Chem Soc* 139:13117-13125.
109. Widdifield CM, Schurko RW (2009) Understanding chemical shielding tensors using group theory, MO analysis, and modern density-functional theory. *Concepts Magn Reson Part A* 34A:91-123.
110. Bochmann M (1996) Cationic group 4 metallocene complexes and their role in polymerisation catalysis: the chemistry of well defined Ziegler catalysts. *Dalton Trans* 0:255-270.
111. Eisenstein O, Jean Y (1985) Factors favoring an M...H-C interaction in metal-methyl complexes. An MO analysis. *J Am Chem Soc* 107:1177-1186.
112. Clot E, Eisenstein O, Agostic Interactions from a Computational Perspective: One Name, Many Interpretations. In *Principles and Applications of Density Functional Theory in Inorganic Chemistry II*, Springer Berlin Heidelberg: Berlin, Heidelberg, 2004; pp 1-36.
113. Brookhart M, Green MLH, Parkin G (2007) Agostic interactions in transition metal compounds. *Proc Natl Acad Sci* 104:6908-6914.

Acknowledgments

CPG is supported by SNF grant number 200020_149704 and is a recipient of the Scholarship Fund of the Swiss Chemical Industry. SS thanks the Osaka University Scholarship for Overseas Research Activities 2017. KY thanks the Canon foundation for a post-doctoral fellowship. OE was partially supported by the Research Council of Norway through its Centres of Excellence scheme, project number 262695. This work is dedicated to the memory of K. Morokuma and T. Ziegler for their contribution to the understanding of the role of organometallic compounds in catalysis; they taught us a lot.

Figures

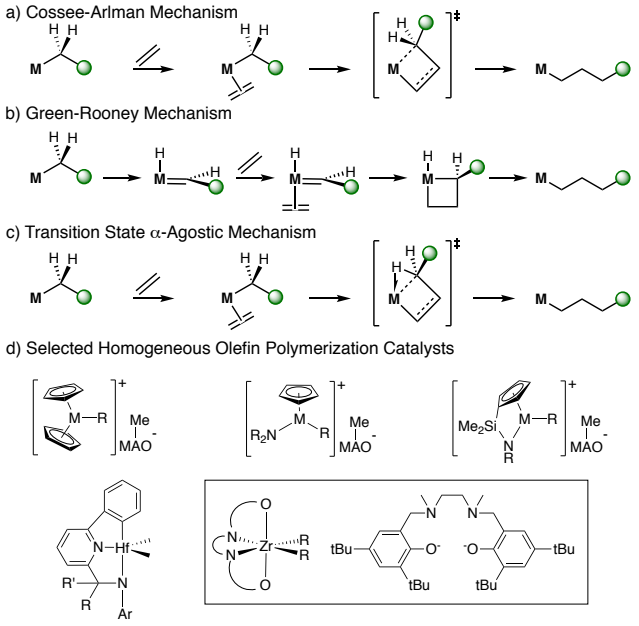

Fig. 1. Proposed mechanisms for olefin insertion involving electrophilic metal centers: a) Cossee-Arlman mechanism, b) Green-Rooney mechanism, and c) modified Green-Rooney mechanism. d) Typical olefin polymerization catalysts (M = Ti, Zr, Hf) (13, 27-31).

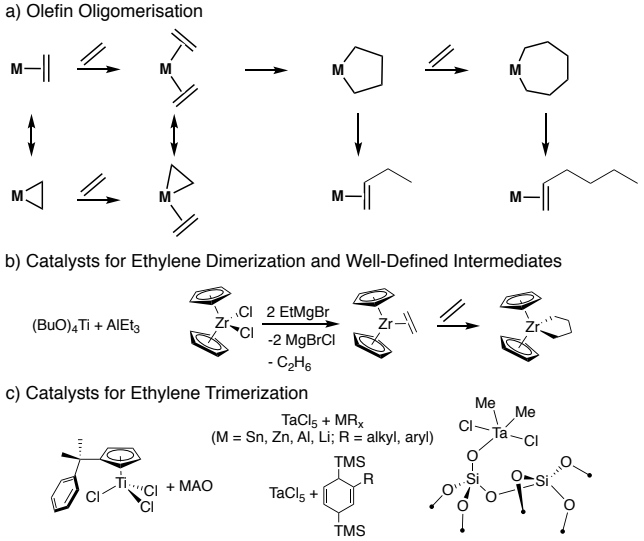

Fig. 2. a) Proposed metallacycle mechanism of olefin oligomerization with early transition-metals, b) catalyst for the dimerization of ethylene and Zr-based model systems, c) selected catalysts for the trimerization of ethylene.

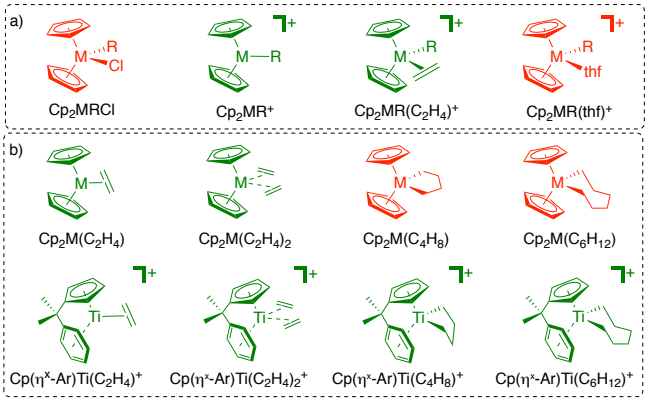

Fig. 3. Analyzed systems related to a) olefin polymerization and b) olefin oligomerization with M = Ti, Zr, Hf and R = Me, Et, Bu. The notation (η^x-Ar) indicates, that the arene-ligand can adopt various coordination modes. The compounds colored in green are active towards olefins, while those in red are not. The chemical shifts (δ_{iso}, δ_{11}, δ_{22}, δ_{33}) for all analyzed Zr-based compounds related to olefin polymerization are shown in Table 1, along with selected Ti and Hf derivatives. The data for Ti-based compounds related to olefin oligomerization and selected Zr compounds are summarized in Table 2. Good agreement between calculated and experimental values is obtained, when data are available. A complete list of all calculated compounds is given in Table S1.

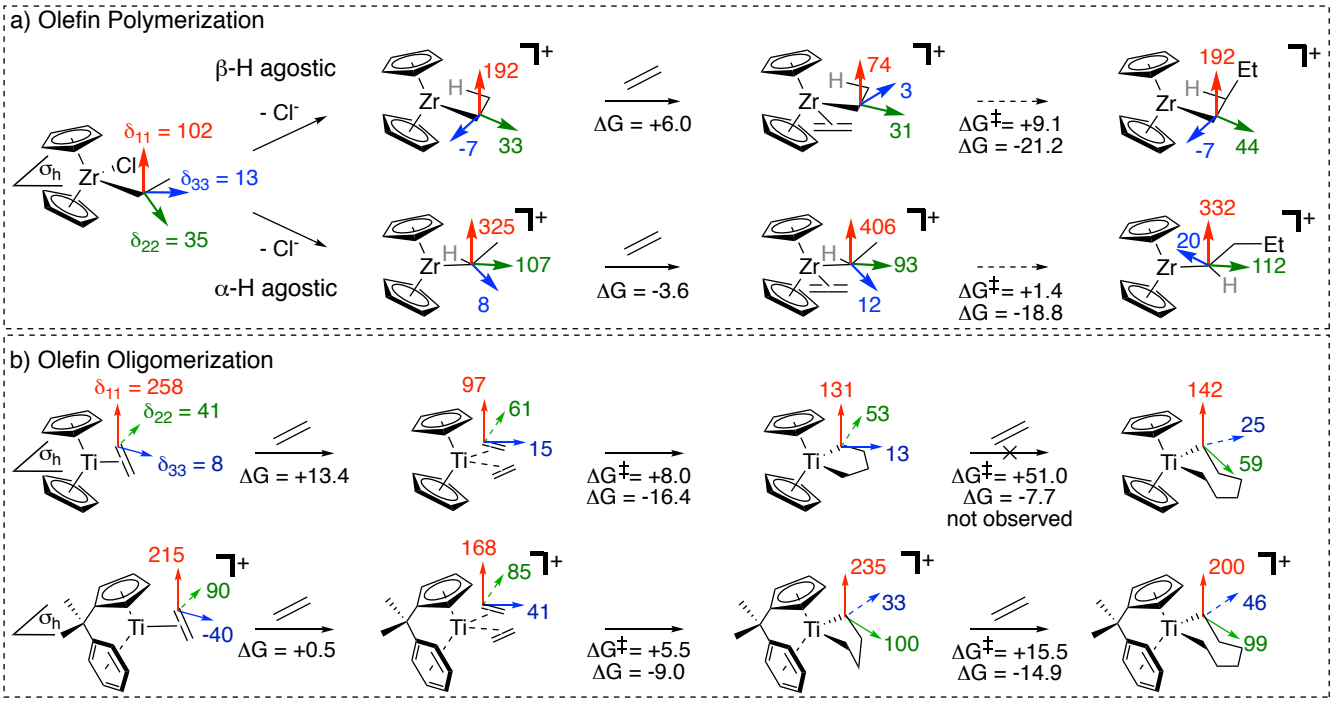

Fig. 4. a) Orientation of the CST for the α-carbon of $Cp_2ZrEtCl$ and the related β-H and α-H (grey coded) agostic cationic Cp_2ZrEt^+ complexes, the ethylene adducts $Cp_2ZrEt(C_2H_4)^+$ and the butyl complexes Cp_2ZrBu^+. The Gibbs energies of activation are calculated for the lowest transition state featuring the respective agostic interaction. The dashed arrow indicates that the two molecules are not directly linked by olefin insertion, and that the product needs to undergo a conformational change to yield the indicated structure. b) Orientation of the CST for systems relevant for ethylene oligomerization. The principal component values (δ_{ii}) of the chemical shift tensors are given in ppm. All Gibbs energies correspond to the reaction step as shown and are given in kcal mol^{-1}.

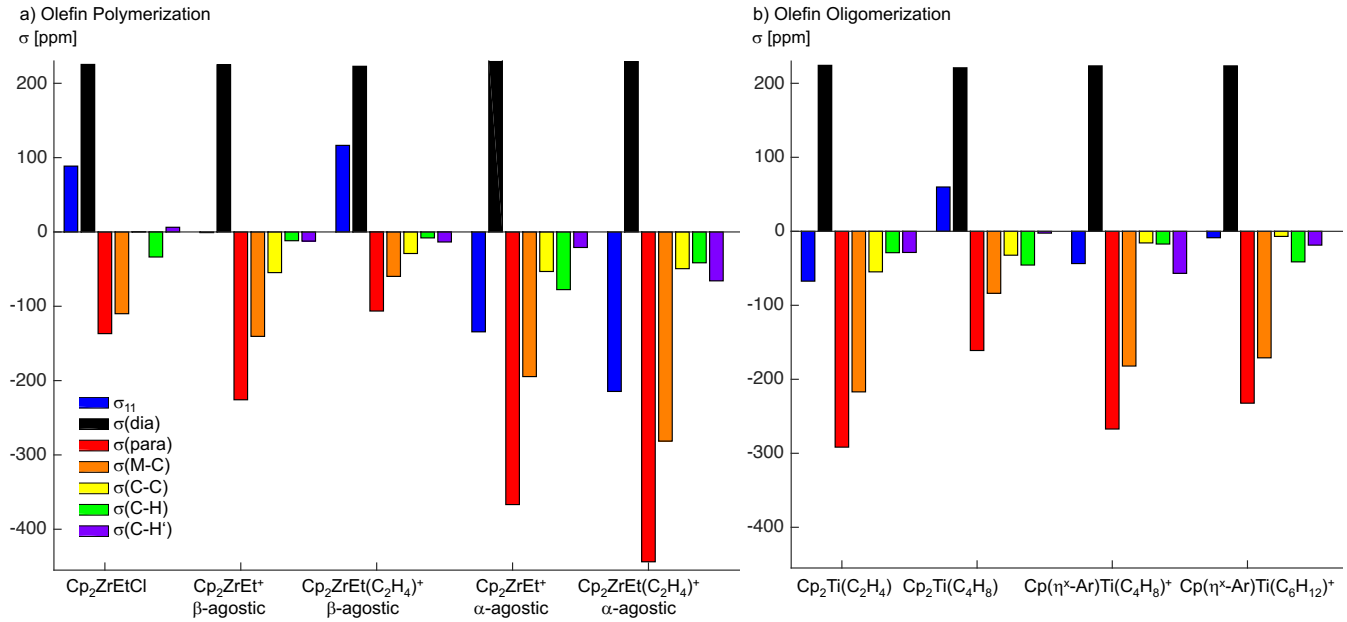

Fig. 5. NCS analysis of the σ_{11} component of the CST in a) Cp_2Zr derived compounds related to olefin polymerization and b) Cp_2Ti and $Cp(\eta^x\text{-}Ar)Ti^+$ derived compounds related to olefin oligomerization.

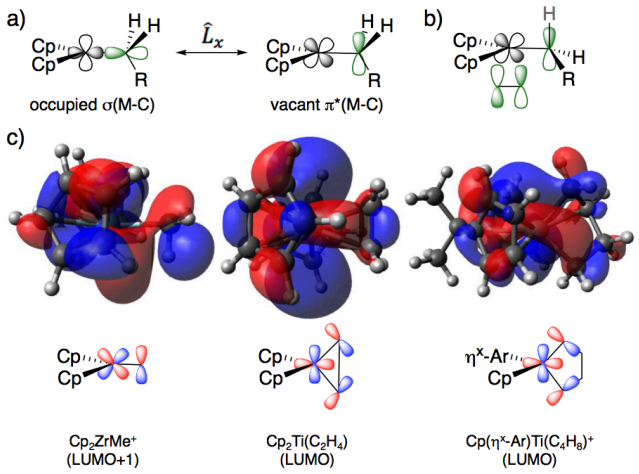

Fig. 6. a) Magnetically induced orbital couplings that gives rise to deshielding of the α-carbon. b) Orbital interaction of the M–C bond with the olefin π*(C=C) orbital, lowering the energy of π*(M–C). c) Calculated and schematic vacant orbitals of π*(M–C) character constructed from a vacant metal d-orbital and contributions from the α-carbons.

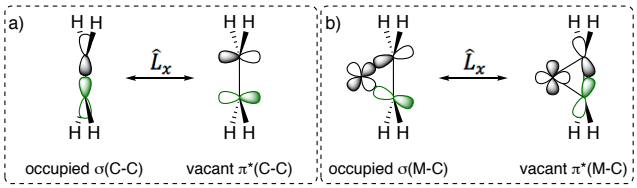

Fig. 7. Magnetically induced orbital couplings responsible for deshielding in a) ethylene and b) $Cp_2M(C_2H_4)$ (M = Ti, Zr, and Hf).

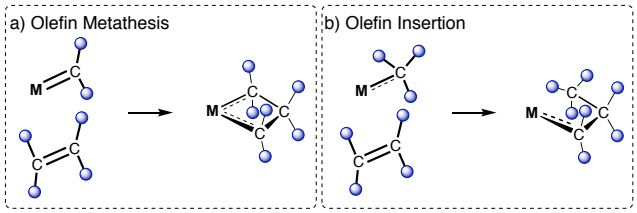

Fig. 8. Parallels between olefin metathesis and olefin insertion.

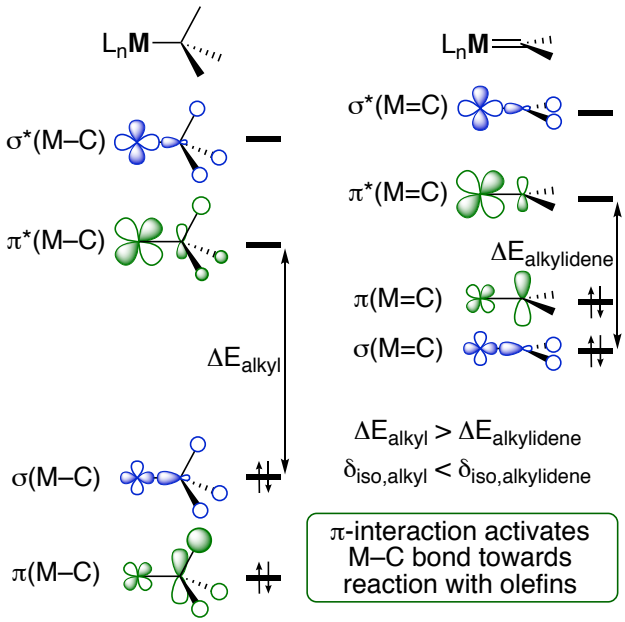

Fig. 9. Qualitative frontier orbital diagram for compounds active towards olefin insertion (left) and olefin metathesis (right). Both species feature a π-interaction between the metal and the α-carbon. ΔE is the energy difference between the σ(M–C) and π*(M–C) orbitals and corresponds to the denominator in eq. 3. Examples of L_nM fragments are Cp_2M or T-shaped $X_2M(=NR)$.

Tables

Table 1. ^{13}C NMR chemical shifts (δ_{iso}, δ_{11}, δ_{22}, δ_{33}) of α-carbons of selected compounds relevant for olefin polymerization processes. Calculated values are given in parenthesis.

Compound	δ_{iso}	δ_{11}	δ_{22}	δ_{33}
$Cp_2TiEtCl$	66 (69)	132 (134)	51 (48)	11 (25)
$Cp_2ZrEtCl$	49 (50)	98 (102)	38 (35)	10 (13)
$Cp_2HfEtCl$	46 (53)	100 (108)	21 (35)	17 (16)
Cp_2ZrMe^+	(101)	(256)	(63)	(-15)
$Cp_2ZrMe(thf)^+$	38 (51)	104 (134)	20 (30)	-10 (-11)
Cp_2ZrEt^+ β-H agos.	61[a] (73)	(192)	(33)	(-7)
Cp_2ZrEt^+ α-H agos.	(147)	(325)	(107)	(8)
Cp_2ZrBu^+ β-H agos.	(76)	(192)	(44)	(-7)
Cp_2ZrBu^+ α-H agos.	(155)	(332)	(112)	(20)
$Cp_2ZrEt(C_2H_4)^+$ β-H agos.	(36)	(74)	(31)	(3)
$Cp_2ZrEt(C_2H_4)^+$ α-H agos.	(172)	(406)	(93)	(12)

[a] reported value for $[(C_5H_4Me)_2ZrEt(thf)][BPh_4]$ in ref. (61)

Table 2. ^{13}C NMR chemical shifts (δ_{iso}, δ_{11}, δ_{22}, δ_{33}) of α-carbons of selected compounds relevant for olefin oligomerization processes. Calculated values are given in parentheses.

Compound	δ_{iso}	δ_{11}	δ_{22}	δ_{33}
$Cp_2Ti(C_2H_4)$	(102)	(258)	(41)	(8)
$(Cp^*)_2Ti(C_2H_4)$	104 (101)	246 (248)	32 (44)	32 (11)
$(Cp)_2Ti(C_2H_4)_2$	(57)	(97)	(61)	(15)
$Cp_2Ti(C_4H_8)$	(66)	(131)	(53)	(13)
$Cp_2Ti(C_6H_{12})$	(75)	(142)	(59)	(25)
$Cp_2Zr(C_2H_4)$	(87)	(235)	(30)	(-5)
$Cp_2Zr(C_4H_8)$	40 (46)	83 (99)	35 (38)	3 (1)
$Cp(\eta^x\text{-}Ar)Ti(C_2H_4)^+$	(89)	(215)	(90)	(-40)
$Cp(\eta^x\text{-}Ar)Ti(C_2H_4)_2^+$	(98)	(168)	(85)	(41)
$Cp(\eta^x\text{-}Ar)Ti(C_4H_8)^+$	(122)	(235)	(100)	(33)
$Cp(\eta^x\text{-}Ar)Ti(C_6H_{12})^+$	(115)	(200)	(99)	(46)
C_2H_4[a]	126 (132)	234 (258)	120 (124)	24 (14)

[a] reported in ref. (62)